Prediction of Brownian particle deposition in porous media using the constricted tube model

You-Im Chang,[a,*] Shan-Chih Chen,[b] and Eric Lee[b]

[a] *Department of Chemical Engineering, Tunghai University, Taichung 40704, Taiwan, Republic of China*
[b] *Department of Chemical Engineering, National Taiwan University, Taipei 10617, Taiwan, Republic of China*

Abstract

The deposition of colloidal particles onto the collector surfaces of porous media is investigated using the Brownian dynamics simulation method. The pore structure in a filter bed was characterized by the constricted tube model. The effects of various shapes of the total interaction energy curves of DLVO theory and the effects of different particle diameters on the collection efficiencies of particles are examined. The simulation results show that the particle collection efficiency is strongly dependent on the geometry of the tube and on the shape of the total interaction energy curve. In a comparison with the available experimental measurements of the filter coefficient, it is found that the present model can give a smaller discrepancy than that of the convective diffusion model in the unfavorable deposition region.
© 2003 Elsevier Inc. All rights reserved.

Keywords: Deposition; Brownian particle; DLVO theory; Porous media

1. Introduction

Granular filtration is a useful fluid–solid separation process for removing various sizes of colloidal particles from fluids—for example, the removal of hydrosols from water treatment and aerosols from gas. When colloidal particles are transported through the porous media of a filter bed, the complicated interactions between the surfaces of particles and the granular collectors are the most important factors to be considered [1]. The method of trajectory analysis [2], which takes into account the molecular dispersion and electrokinetic and hydrodynamic forces, is a useful tool to describe the deposition behavior of colloidal particles on the collector surfaces, by adopting the concept of the limiting trajectory [3]. In this trajectory method, in order to properly describe the hydrodynamic flow field around the collector surface, a number of different unit cell models are adopted to describe the geometry of pore structure in the porous media, such as (a) the capillary tube model [4,5], (b) the single sphere model [6–8], (c) the sphere-in-cell model [3,9,10], and (d) the constricted tube model established by Payatakes et al. [11]. Among which, the constricted

tube model is the only model takes the joint effect of neighboring grains and the shape and size of the nodes connecting pores into consideration. So the constricted tube model is adopted for modeling the porous media in the present paper.

Also, the Brownian diffusion force was not considered in earlier works of trajectory analysis; hence the force balance equations obtained in these analyses were deterministic. However, when Brownian diffusion is the dominant force of the deposition process, the deterministic calculation of particle trajectory is no longer possible. Inclusion of these Brownian random forces in this Lagrangian type force balance equation leads to a Langevin type equation, which was solved successfully by Kanaoka et al. [12] in their simulation model of the aerosol filtration. This Brownian dynamics simulation method proved to be useful when the inertia and long-range forces (i.e., van der Waals attraction and electrical double layer repulsion) are of the same order as the Brownian diffusion force [13,14]. Combining the concept of control window with this dynamics method, a stochastic procedure was established successfully in our previous papers to simulate the initial deposition behavior of colloidal particles [15,16]. In these papers, the effect of various shapes of the total interaction energy curve of DLVO theory [17] on the collection efficiency of colloidal particles was simulated by adopting the Kuwabara cell model. And the results show

* Corresponding author.
 E-mail address: yichang@mail.thu.edu.tw (Y.-I. Chang).

that the height of the primary maximum and the depth of the secondary minimum in the total interaction energy curve play important roles in determining the collection efficiency of Brownian particles at low Reynolds numbers.

In the first part of this paper, in order to investigate the effect of wall geometry on the deposition rates of Brownian particles, the parabolic constricted tube (PCT), the sinusoidal constricted tube (SCT), and the hyperbolic constricted tube (HCT) are adopted in the Brownian dynamics simulation method. In these simulations, the effects of the various shapes of the total interaction energy curves and the effects of the particle diameter are also considered. Theoretical predictions obtained by the present model are compared with experimental data reported by Elimelech and O'Melia [18], as well as by Bai and Tien [19]. Furthermore, results obtained with the previous convective diffusion model [20] are presented in the second part of this paper.

2. The constricted tube model

In this model, the filter bed is considered to be composed of a number of unit bed elements (UBE) connected in series. The unit bed elements are uniform in thickness and are statistically similar. Each unit bed element contains a number of unit cells of the shape of the constricted tube with a given size distribution. To simplify the analysis, these unit cells contained in a UBE are assumed to be of the same size in the present study. The dimension of the constricted tube is characterized by three quantities: the height, h, the maximum diameter, d_{max}, and the constriction diameter, d_c. The radius r_c and r_{max} are $d_c/2$ and $d_{max}/2$, respectively. Expressions for the determination of these quantities are summarized in Table 1. A schematic representation is shown in Fig. 1. For a spherical collector with diameter d_f, the relationship between r_c, r_{max}, and d_f is defined as [2]

$$r_c = \frac{d_c}{2} = \frac{1}{2}\frac{\langle d_c \rangle}{\langle d_f \rangle} d_f, \tag{1}$$

$$r_{max} = \frac{d_{max}}{2} = \frac{1}{2}\left[\frac{\varepsilon(1-S_{wi})\langle d_f^3 \rangle}{(1-\varepsilon)\langle d_c^3 \rangle}\right]^{1/3} d_f, \tag{2}$$

Table 1
Summary of expressions for porous media characterization based on the constricted tube model

Quantity	Expression
Length of periodicity, l_f	$\left[\dfrac{\pi}{6(1-\varepsilon)}\right]^{1/3}\langle d_f \rangle$
Number of unit cells per unit bed element, N_c	$\dfrac{6\varepsilon(1-S_{wi})}{\pi\langle d_c^3 \rangle}\left[\dfrac{\langle d_c \rangle - \varepsilon\langle d_c^3 \rangle}{\varepsilon(1-S_{wi})\langle d_c^3 \rangle}\right]^{2/3}$
Height, h	d_f
Minimum diameter, d_c	$\dfrac{\langle d_c \rangle}{\langle d_f \rangle}d_f$
Maximum diameter, d_{max}	$\left[\dfrac{\varepsilon(1-S_{wi})\langle d_f^3 \rangle}{(1-\varepsilon)\langle d_c^3 \rangle}\right]^{1/3} d_c$
Volumetric flow rate in a given type of unit cell, q_i	$\dfrac{u_s}{N_c}$

where ε denotes the porosity of porous media, $\langle d_f \rangle$ and $\langle d_c \rangle$ are the mean values of the diameter of spherical collectors and pore constrictions, respectively, and $\langle d_f^3 \rangle$ and $\langle d_c^3 \rangle$ are the mean values of d_f^3 and d_c^3, respectively. In Eq. (2), S_{wi} represents the fraction of the irreducible saturation of porous media, and its value is 0.111 for glass bead collectors and 0.127 for sand grain collectors [11]. In the present study, the filtration bed is assumed to be packed with sand grains.

Three different geometric structures are considered for the constricted tube model in the present study: the parabolic geometry (PCT as parabolic constricted tube) used by Payatakes et al. [11] in their original formulation, and two subsequent models of the sinusoidal (SCT) and hyperbolic (HCT) geometry considered by Fedkiw and Newman [21] and Venkatesan and Rajagopalan [22], respectively. The expressions for the wall radius r_w corresponding to these three geometric structures are given in Table 2. With the assumed values for a filter bed given in Table 3, the schematic diagrams of these three constricted tube models are shown in Fig. 2, with which $d_{max} = 80$, $d_c = 36$, and $h = 100$ μm. From these three geometric structures, it can be found that the tube wall of PCT exhibits the highest slope at the en-
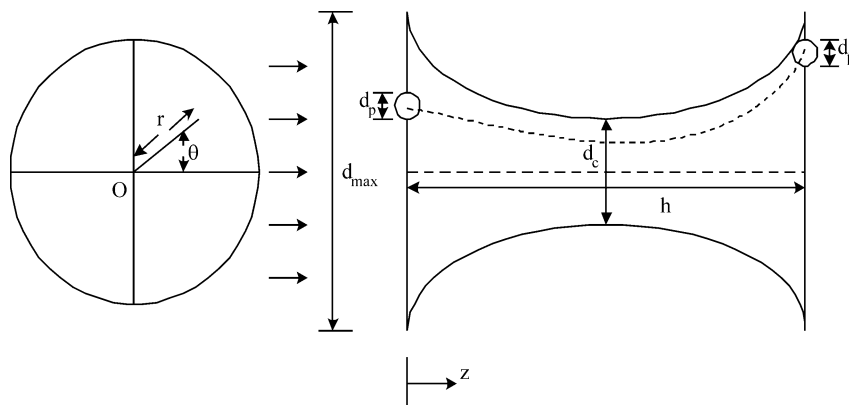
Fig. 1. The schematic diagram of the control window for simulating deposition of Brownian particles in a constricted tube model.

Table 2
Equations describing the wall geometry for different types of the constricted tube structure

PCT (parabolic constricted tube)

$$r_w = r_c + 4(r_{max} - r_c)\left(0.5 - \frac{z}{l_f}\right)^2 \quad \text{for } 0 < \frac{z}{l_f} < 1,$$

SCT (sinusoidal constricted tube)

$$r_w = \frac{r_c + r_{max}}{2}\left[1 + \left(\frac{r_{max} - r_c}{r_{max} + r_c}\right)\cos\left(2\pi\frac{z}{l_f}\right)\right],$$

HCT (hyperbolic constricted tube)

$$r_w = (1 - \zeta_0^2)^{1/2}\left[\alpha_0^2 + \frac{(z/l_f - 0.5)^2}{\zeta_0^2}\right]^{1/2},$$

where

$$\zeta_0 = \left\{4r_c^2\left[\left(\frac{r_{max}}{r_c}\right)^2 - 1\right] + 1\right\}^{-1/2},$$

$$\alpha_0 = \frac{\{4r_c^2[(r_{max}/r_c)^2 - 1] + 1\}^{1/2}}{2[(r_{max}/r_c)^2 - 1]^{1/2}}.$$

Table 3
Parameter values adopted in the theoretical simulation of the present paper

Parameters	Ranges
N_{E1}	0–10^3
N_{E2}	-1–1
N_{LO}	10^{-3}–10^2
N_{DL}	5–10^2
k_B	1.38×10^{-16} erg K^{-1}
ε	0.39
μ	1 cp
T	293 K
ρ_f	1.0 g cm^{-3}
ρ_p	2.5 g cm^{-3}
d_f	100 µm
d_p	1 µm
S_{wi}	0.111

trance and the lowest slope at the constriction part of the tube, and *vice versa* for SCT. The flow fields corresponding to these three geometric structures are different. For example, for SCT, the streamlines at the entrance of the unit cell are parallel to the axial direction, and persist along that direction over a certain distance before they move toward the center of the tube. This puts particles in a more favorable situation for collection than that of a PCT, at which the streamlines at the entrance are parallel to the axis, but change their direction very quickly as they move into the cell center [23]. In the present study, the flow field equations established by Chow and Soda [24] and modified by Chiang and Tien [25] are adopted, which is briefly described as follows.

By assuming the wall radius r_w as an arbitrary function of the axial distance in the constricted tube, the stream function of flow can be expressed as

$$\psi^* = \frac{\psi}{u_m r_m^2} = \psi_0^* + R_m\psi_1^* + R_m^2\psi_2^*, \tag{3}$$

at which the zeroth, first, and second order solutions of stream functions are given, respectively, as

$$\psi_0^* = 0.5(R^4 - 2R^2), \tag{4}$$

$$\psi_1^* = 0.25 N_{Re,m}\frac{dR_w/dZ}{R_w}\left[\frac{1}{9}(R^8 - 6R^6 + 9R^4 - 4R^2)\right], \tag{5}$$

$$\psi_2^* = -0.5\left[5\left(\frac{dR_w}{dZ}\right)^2 - R_w\frac{d^2R_w}{dZ^2}\right]\frac{(R^2 - 1)^2 R^2}{3}$$
$$- 0.125 N_{Re,m}\left(\frac{dR_w/dZ}{R_w}\right)^2$$
$$\times\left[32R^{12} - 305R^{10} + 750R^8 - 713R^6 + 236R^4\right]/3600, \tag{6}$$

where

$$Z = z/l_f, \qquad R_w = r_w/r_m, \qquad R = r/r_w,$$

$$R_m = r_m/l_f, \qquad r_m = \frac{1}{l_f}\int_0^{l_f} r_w\, dz, \qquad N_{Re,m} = \frac{u_m r_m \rho_f}{\mu}.$$

The relationship between u_m and the superficial velocity through the filter bed, u_s, is

$$u_s = (u_m)(\pi r_m^2)N_c, \tag{7}$$

where N_c is the number of the constricted tubes per unit cross section of the bed, and its definition is given in Table 1.

The expressions of the velocity components u_r and u_z are

$$u_r = u_m\left(u_{r0}^* + R_m u_{r1}^* + R_m^2 u_{r2}^*\right)\frac{r_m^2}{r_w l_f}, \tag{8}$$

$$u_z = u_m\left(u_{z0}^* + R_m u_{z1}^* + R_m^2 u_{z2}^*\right)\frac{r_m^2}{r_w^2}, \tag{9}$$

where the zeroth, first, and second order dimensionless expressions of the two components u_r and u_z are given, respectively, as

$$u_{r0}^* = -2\frac{dR_w/dZ}{R_w}(R^3 - R), \tag{10}$$

$$u_{r1}^* = \frac{0.25}{R}N_{Re,m}\left\{F\left[\frac{d^2R_w/dZ^2}{R_w} - \left(\frac{dR_w/dZ}{R_w}\right)^2\right]\right.$$
$$\left. + \frac{dF}{dZ}\frac{dR_w/dZ}{R_w}\right\}, \tag{11}$$

$$u_{r2}^* = -0.5\left\{\left(9\frac{dR_w}{dZ}\frac{d^2R_w}{dZ^2} - R_w\frac{d^3R_w}{dZ^3}\right)\frac{G}{R}\right.$$
$$\left. + \left[5\left(\frac{dR_w}{dZ}\right)^2 - R_w\frac{d^2R_w}{dZ^2}\right]\frac{dG}{R\,dZ}\right\}$$
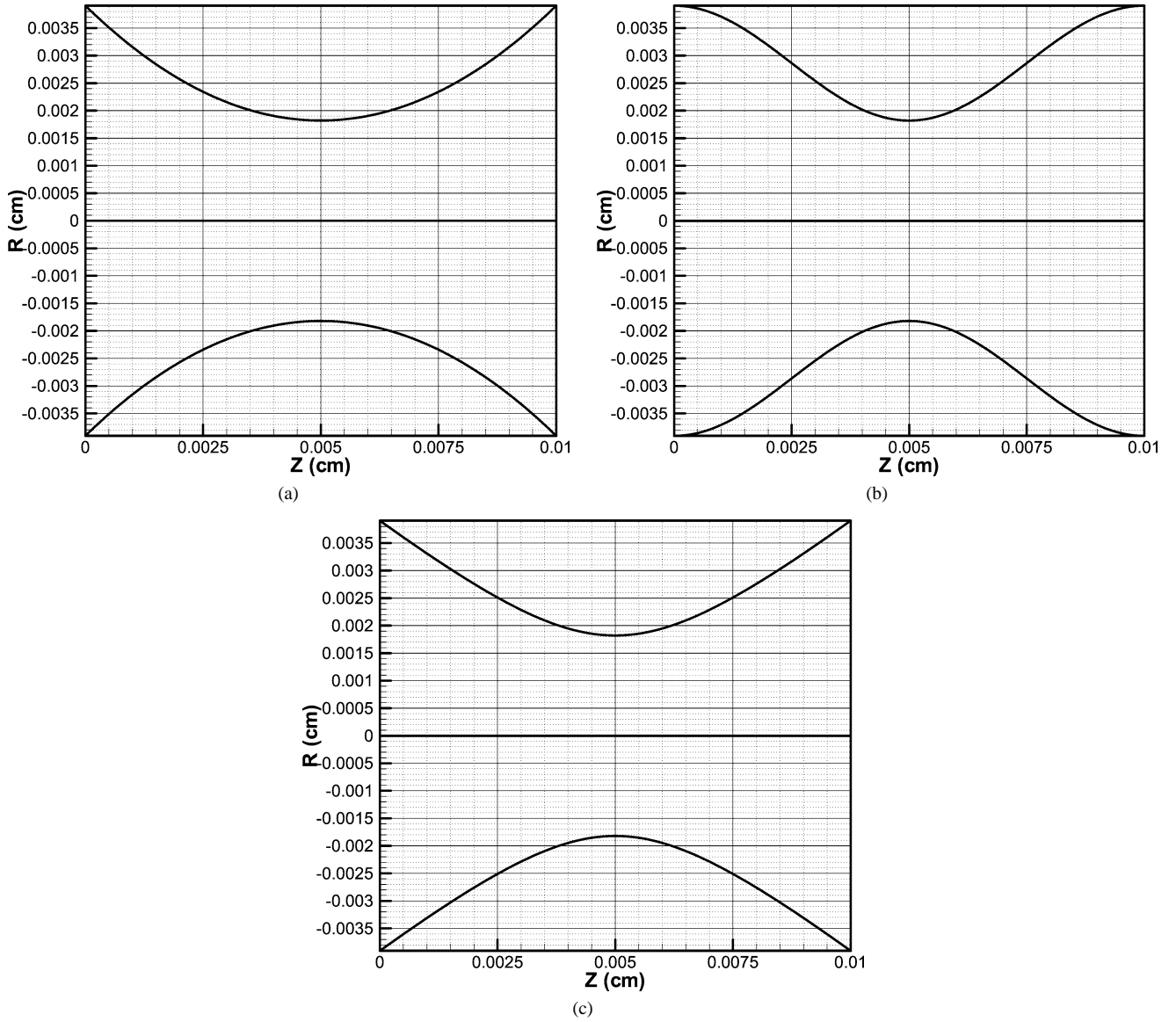
Fig. 2. Geometric figures of three different constricted tube structures adopted in the present paper, at which $d_{max} = 80$, $d_c = 36$, and $h = 100$ μm: (a) the parabolic constricted tube (PCT); (b) the sinusoidal constricted tube (SCT); (c) the hyperbolic constricted tube (HCT).

$$- 0.125 N_{Re,m} \left\{ 2 \frac{dR_w/dZ}{R_w} \left[\frac{d^2 R_w/dZ^2}{R_w} \right. \right.$$

$$\left. \left. - \left(\frac{dR_w/dZ}{R_w} \right)^2 \right] \frac{E}{R} + \left(\frac{dR_w/dZ}{R_w} \right)^2 \frac{dE}{RdZ} \right\}, \quad (12)$$

$$u_{z0}^* = 2 \left(1 - R^2 \right), \quad (13)$$

$$u_{z1}^* = - \frac{0.25}{R} N_{Re,m} \frac{dF}{dR} \frac{dR_w/dZ}{R_w}, \quad (14)$$

$$u_{z2}^* = 0.5 \left[5 \left(\frac{dR_w}{dZ} \right)^2 - R_w \frac{d^2 R_w}{dZ^2} \right] \frac{dG}{RdR}$$

$$+ 0.125 N_{Re,m} \left(\frac{dR_w/dZ}{R_w} \right)^2 \frac{dE}{RdR}, \quad (15)$$

where

$$F = \left(R^8 - 6R^6 + 9R^4 - 4R^2 \right) / 9,$$

$$G = \left(R^2 - 1 \right) R^2 / 3,$$

$$E = \left(32R^{12} + 305R^{10} + 750R^8 - 713R^6 + 236R^4 \right) / 3600.$$

3. Simulation procedure

Similar to the previous papers of Ramarao et al. [14] and authors [15,16], the principle of trajectory analysis and the concept of control window are adopted in the present simulation. Assume that the distribution of the initial position (r_{in}, θ_{in}) of each approaching particle of the same size is

assigned by the random number generator in the flow field simulation. Note that the inlet positions of particles are located at $0 < r_{in} < r_0$ and $0 < \theta_{in} < 2\pi$ (see Fig. 1), at which r_0 is the radial distance beyond which no particle can be placed at the tube inlet (or control window), and r_0 can be found to be

$$r_0 = \frac{d_{max} - d_p}{2}. \qquad (16)$$

With consideration of the inertia term in the force balance equation and of the specification of the flow fluid around the collector, the particle trajectory can be determined by integrating the Langevin equation as shown below.

The particle velocity vector is represented as

$$V = \left\{ \left[V_0 e^{-\beta t} + U(1 - e^{-\beta t}) \right] F_2(H) + R_v(t) \right.$$
$$\left. + \frac{1}{\beta} \left(\frac{F_{LO} + F_{DL}}{m_p} \right) (1 - e^{-\beta t}) \right\} F_1(H) F_3(H) \qquad (17)$$

with

$$R_v(t) = \int_0^t e^{\beta(\zeta - t)} A(\zeta) \, d\zeta,$$

where V_0 is the initial velocity of particles, m_p is the mass of the particle, U is the fluid velocity vector, β is the friction coefficient per unit mass of particle, and $F_1(H)$, $F_2(H)$, and $F_3(H)$ are the retardation factors of normal vector, drag force, and shear vector, respectively [3]. Substituting dZ/dt for V with the initial condition $S = S_0$ at $t = 0$, the trajectory equation of particles can be expressed as

$$Z = Z_0 + \left\{ \frac{V_0}{\beta} (1 - e^{-\beta t}) + U \left[t - \frac{1}{\beta} (1 - e^{-\beta t}) \right] \right\}$$
$$\times F_1(H) F_2(H) F_3(H)$$
$$+ \left\{ R_r(t) + \left(\frac{F_{LO} + F_{DL}}{\beta m_p} \right) \left(t + \frac{e^{-\beta t}}{\beta} - \frac{1}{\beta} \right) \right\}$$
$$\times F_1(H) F_3(H), \qquad (18)$$

with

$$R_r(t) = \int_0^t \left[\int_0^n e^{\beta \zeta} A(\zeta) \, d\zeta \right] e^{-\beta n} \, dn,$$

where $A(t)$ represents a Gaussian white noise process in stochastic terms. $R_v(t)$ and $R_r(t)$ are two random deviates which are bivariate Gaussian distribution. The details of $R_v(t)$ and $R_r(t)$ can be found in Kanaoka et al. [12] and Ramarao et al. [14].

In Eqs. (17) and (18), F_{LO} and F_{DL} are the van der Waals force and the electrostatic repulsion force interacting between the particle and the collector surface, respectively;

$$F_{LO} = -\nabla \phi_{LO}, \qquad F_{DL} = -\nabla \phi_{DL} \qquad (19)$$

with

$$\phi_{LO} = -N_{LO} \left[\frac{2(H+1)}{H(H+2)} + \ln H - \ln(H+2) \right]$$

(with the unit of $k_B T$)

$$\phi_{DL} = N_{E1} \left\{ N_{E2} \ln \left[\frac{1 + \exp(-X)}{1 - \exp(-X)} \right] + \ln \left[1 - \exp(-2X) \right] \right\}$$

(with the unit of $k_B T$);

hence

$$F_{LO} = -\frac{2A}{3r_p} \left[\frac{1}{(H^2 + 2H)^2} \right], \qquad (20)$$

$$F_{DL} = \frac{2k_B T}{r_p} N_{E1} \left(N_{DL} e^{-N_{DL} H} \right) \left\{ \frac{N_{E2} - e^{-N_{DL} H}}{1 - e^{-2N_{DL} H}} \right\}, \qquad (21)$$

where

$$H = \frac{h_s}{r_p}, \qquad N_{LO} = \frac{A}{6k_B T}, \qquad N_{DL} = \kappa r_p,$$
$$X = N_{DL} H,$$
$$N_{E1} = \frac{\nu r_p (\varphi_1^2 + \varphi_2^2)}{4k_B T}, \qquad N_{E2} = \frac{2 \left(\frac{\varphi_1}{\varphi_2} \right)}{\left[1 + \left(\frac{\varphi_1}{\varphi_2} \right)^2 \right]}.$$

In the above equation, h_s is the smallest separation distance between the particle and the collector surface, A is the Hamaker constant, k_B is the Boltzmann constant, T is the absolute temperature, κ is the reciprocal of the electric double layer thickness, ν is the dielectric constant of the fluid, and φ_1 and φ_2 are the surface (zeta) potentials of the particle and the collector, respectively. The algebraic sum of the van der Waals and double-layer potentials gives the total interaction energy curve of the DLVO theory (i.e., $V_T/k_B T = \phi_{LO} + \phi_{DL}$). In this total interaction energy profile, the existence of two characteristic energy barriers (i.e., the height of the primary maximum and the depth of the secondary minimum) is important in determining the collection efficiency η_s as discussed below.

From the trajectory of a given particle, one can then determine whether this particle will deposit on the collector or not. With these simulation steps, the single collector collection efficiency describing the initial deposition rate of Brownian particles can be defined as [14]

$$\eta_s = \left(\frac{y_0}{r_f} \right) P(y_0) \quad \text{with } P(y_0) = \frac{N_{dep}}{N_{gen}}, \qquad (22)$$

where N_{gen} is the number of particles entering the control window and N_{dep} is the number of particles deposited. To calculate $P(y_0)$, the value of $N_{gen} = 1000$ and the average value of η_s from 10 trials are used in the present case.

4. Simulation results and their comparisons with experiments

The estimation of the collection efficiency describing particles' initial deposition behavior from the trajectory equa-

tions based on the above stochastic simulation procedures for the different interaction energy curves, and for the different constricted tube structures are given below. The corresponding electrokinetic data and other simulation parameters are given in Table 3. The present simulation is compared with the experimental data reported by Elimelech and O'Melia [18] and by Bai and Tien [19] first, and then with the results of the convective diffusion model [20]. The accuracy of the above simulation method will be discussed in a later section.

4.1. Effect of the interaction force

The effects of the four types of interaction energy curves [26] on the collection efficiencies of Brownian particles will be investigated in the present section. As shown in Fig. 3, curves A exhibits a large primary maximum and a deep secondary minimum; curve B displays a large primary maximum and a negligible secondary minimum; while curve C owns a deep secondary minimum only and a "barrierless" interaction energy curve is represented by curve D. In this figure, $N_{E1} = 105.0$ and $N_{DL} = 10.75$ for curve A, $N_{E1} = 50.0$ and $N_{DL} = 5.02$ for curve B, $N_{E1} = 77.0$ and $N_{DL} = 10.0$ for curve C, $N_{E1} = 0.0$ and $N_{DL} = 0.0$ for curve D, and $N_{E2} = 1.0$ and $N_{LO} = 7.0$ for all four curves. Corresponding to these four types of interaction energy curves with the defined values of N_{E1}, N_{E2}, N_{LO}, and N_{DL} and the three different porous media models (i.e., SCT, HCT, and PCT), the simulation results of the collection efficiencies η_s at various values of Reynolds number (i.e., based on the tube diameter and fluid velocity) are given in Figs. 4a, 4b, and 4c, respectively.
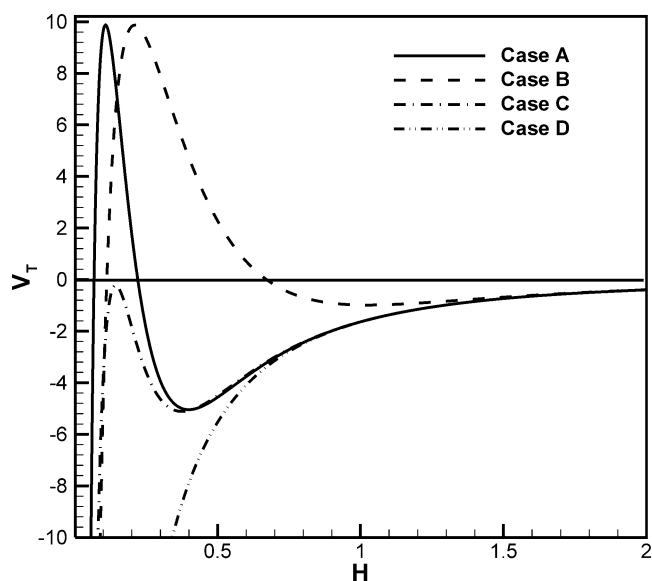
Fig. 3. Four types of total interaction energy curves adopted in the simulation of the present paper, at which $N_{E1} = 105.0$ and $N_{DL} = 10.75$ for curve A, $N_{E1} = 50.0$ and $N_{DL} = 5.02$ for curve B, $N_{E1} = 77.0$ and $N_{DL} = 10.0$ for curve C, $N_{E1} = 0.0$ and $N_{DL} = 0.0$ for curve D, and $N_{E2} = 1.0$ and $N_{LO} = 7.0$ for all four curves.

The simulation results for SCT are shown in Fig. 4a, which indicate that the order of the magnitudes of η_s in general is curve D > curve C > curve B > curve A, with the exception that curve B > curve C when $N_{Re} \geqslant 1.8$. Since no energy barrier exists, the collection efficiencies of curve D are always greater than those of the other three curves, and a maximum is observed at $N_{Re} = 0.3$. Since the deposition mechanism of particles is controlled by the Brownian diffusion effect when $N_{Re} \leqslant 0.3$, as the particle inertia increases, these particles will be more likely to retain their initial direction toward the tube wall at the entrance of the SCT tube. This implies that the capture possibility of particles will become greater with increased Reynolds number. However, when $N_{Re} > 0.3$, the inertial effect becomes dominant and those particles at the entrance will move away from the tube wall toward the center of the tube. Consequently, collection efficiency of particles will decrease with the increase of the particle inertia when $N_{Re} > 0.3$. This explains why there is a maximum in this "barrierless" curve D as shown in Fig. 4a.

Contrary to the decreasing tendency observed in curve D, the values of η_s of curves A, B, and C increase with the increase of N_{Re} as shown in Fig. 4a, because the increased inertia forces can overcome the energy barriers shown in Fig. 3. Comparing curve A with curves B and C, it is found that, even with the presence of the deep secondary minimum which increases the accumulation of particles for curves B and C, the steep slope between the secondary minimum and the primary maximum energy barriers of curve A is still the main reason for its lowest collection efficiency among the three curves. But when $N_{Re} \geqslant 1.8$, because of a greater sweep away probability caused by the tangential fluid convection force acting on those particles accumulating at the secondary minimum, the η_s of curve C is smaller than that of curve B.

As shown in Figs. 4b and 4c, similar results are obtained for PCT and HCT, respectively. The reasons given in Fig. 4a can be drawn to explain these variations observed in these two figures. For PCT and HCT, the maxima of curve D occur at $N_{Re} = 0.7$ and $N_{Re} = 0.4$, respectively. And the inverse of the magnitudes of η_s for curve B and curve C happens at $N_{Re} = 1.2$ and $N_{Re} = 0.7$, respectively. For curve A shown in Figs. 4a, 4b, and 4c, it is interesting to find that, because of its lower slope of the tube wall at the constriction part of the tube, the collection efficiency for either PCT or HCT is almost zero and is much smaller than that of SCT when $N_{Re} \geqslant 1.0$.

When comparing the magnitudes of η_s at different Reynolds numbers among these three tube structures, we found that SCT > HCT > PCT in general for curves A, B, and C, respectively, and *vice versa* for curve D. The illustrative examples for curves B and D are shown in Figs. 5a and 5b, respectively. For curve B in Fig. 5a, since these particles can persist a longer distance at the entrance in the SCT tube, its collection efficiencies of particles are higher than that of HCT and PCT as N_{Re} becomes greater. When $N_{Re} \geqslant 1.50$ (at which the inertia effect becomes dominant),
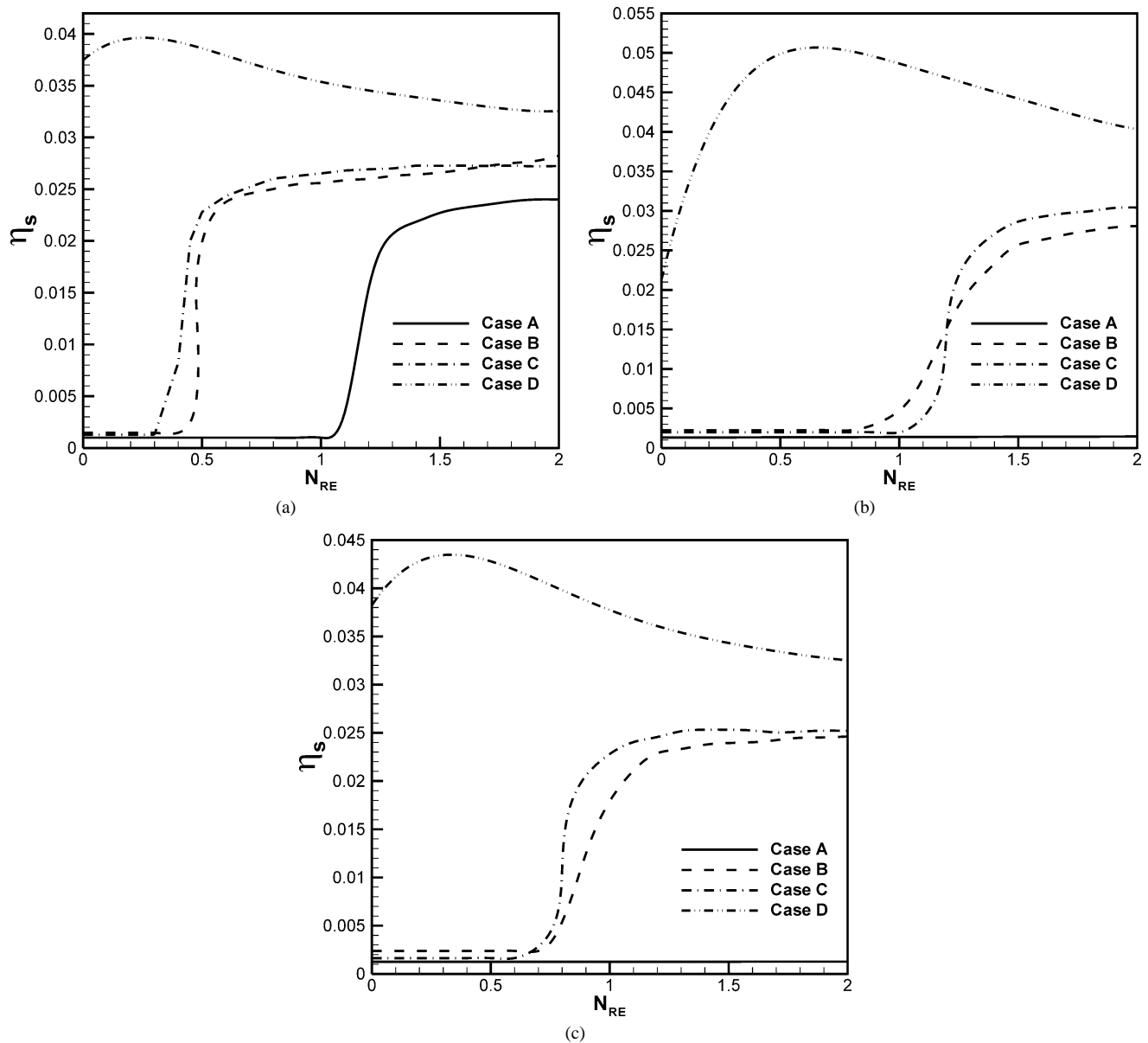
Fig. 4. Simulation results of the collection efficiency η_s versus Reynolds number N_{Re}, corresponding to these three different constricted tube structures described in Fig. 2 and four types of interaction energy curves shown in Fig. 3: (a) simulation results for the SCT model; (b) simulation results for the PCT model; (c) simulation results for the HCT model.

because of its highest slope of the tube wall being at the entrance, the collection efficiency of PCT becomes higher than that of HCT and close to that of SCT. Also, since the particles at the entrance of the tube will collide with the tube wall immediately (see Fig. 1), the collection efficiencies of these three constricted tube structures are much greater than that of the spherical collector model when $N_{Re} \geqslant 1.0$ [15], at which the Kuwabara fluid field model was adopted. Also, as shown in Fig. 5a, the dashed lines represent the simulation results when the well known trajectory equations of the constricted tube model established by Payatakes et al. [11] are adopted, at which the Brownian diffusion deposition mechanism is ignored. It is found that the collection efficiencies of particles obtained by the present work are lower than these

predictions obtained by using the Payatakes model, which indicates that the Brownian diffusion effect exhibits a negative effect on the collection efficiency of particles for this type B interaction energy curve. However, for the barrierless curve D, as shown in Fig. 5b, the Payatakes model's predication is higher than that of the present work, and this difference becomes more profound when the Reynolds number of fluid is small indicating the Brownian diffusion effect is the dominant deposition mechanism. Contrary to these magnitudes of η_s observed in Fig. 5a, as shown in Fig. 5b when N_{Re} is large, the collection efficiency of PCT is the highest among these three tube structures, because of its highest slope of the tube wall being at the entrance. Note that there are no maxima observed for these curves with-

(a)

(b)
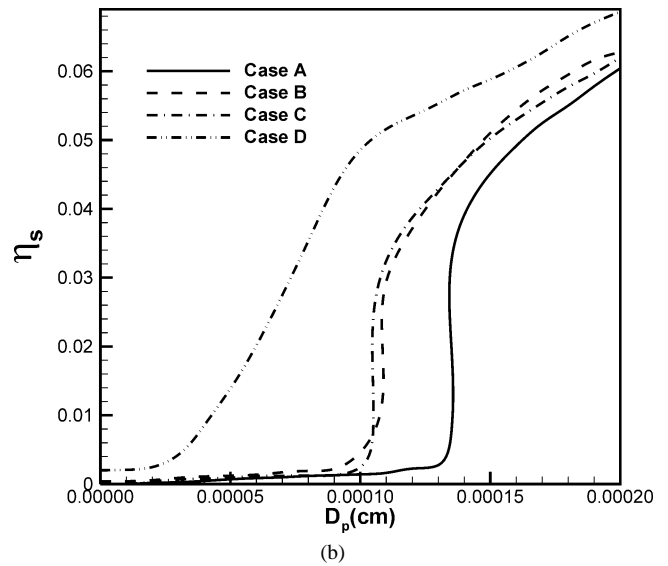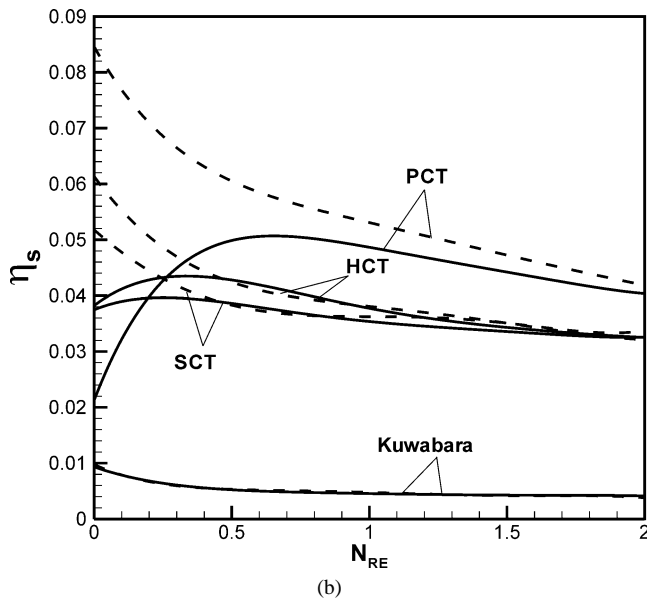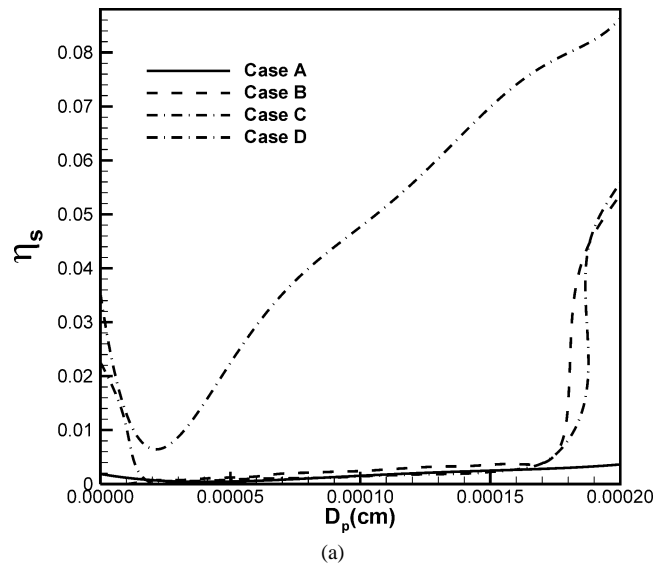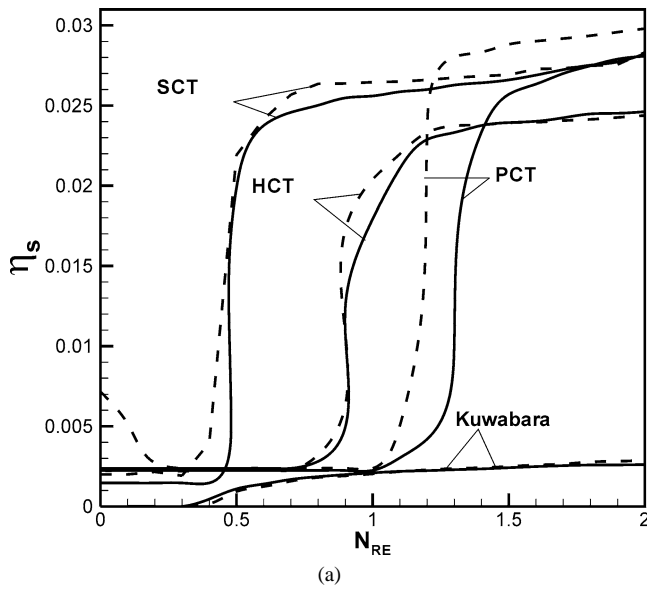
Fig. 5. Simulation results of the collection efficiency η_s versus Reynolds number N_{Re}, corresponding to these three tube structures described in Fig. 2 and the spherical collector model, at which the Kuwabara flow field model is adopted [15]: (a) simulation results for the type B interaction energy curve shown in Fig. 3; (b) simulation results for the type D interaction energy curve shown in Fig. 3. In this figure, solid lines represent the simulation results obtained by using the present Brownian dynamics model, and dashed lines represent the simulation results obtained by using the trajectory model established by Payatakes et al. [11], in which the Brownian diffusion effect is ignored.

out considering the Brownian diffusion effect as shown by dashed lines in Fig. 5b.

4.2. Effect of the particle size

Figure 6a shows the predicted collection efficiency as a function of the particle diameter for the four types of inter-action energy curves, adopting the PCT geometric structure

(a)

(b)

Fig. 6. Simulation results of the collection efficiency η_s versus particle diameter d_p, corresponding to these four types of interaction energy curves shown in Fig. 3 when the PCT model is adopted: (a) simulation results for $N_{Re} = 0.1$; (b) simulation results for $N_{Re} = 1.0$.

and $N_{Re} = 0.1$. For a chosen particle diameter, since there is no energy barrier, the collection efficiency of curve D is the highest. Also, for curve D when $N_{Re} < 0.2$ μm, the collection efficiency of particles decrease, because of the decreased Brownian diffusion effect with the increase of particle diameter. After passing through this minimum at $d_p = 0.2$ μm, the collection efficiency increases rapidly with the increase of particle diameter, at which the inertia force becomes more important and dominates others deposition mechanisms eventually. The same results are obtained for curve C, except that the values of η_s will only increase slightly when 0.2 μm $< d_p < 1.8$ μm, which is caused by the easy accumulation of particles at the deep secondary min-imum of curve C. Because of the existence of the primary maximum energy barrier, the collection efficiency of curve B

is not obvious until $d_p > 1.8$ μm. Since the height of the primary maximum is too high for particles to overcome, the collection efficiency of curve A is almost zero as shown in Fig. 6a. When Reynolds number increase from $N_{Re} = 0.1$ to $N_{Re} = 1.0$, as shown in Fig. 6b, no minimum is observed on either curve C or curve D, because the Brownian diffusion effect is no longer important. Curve D still has the highest collection efficiency among these four types of interaction energy curves, and increases with the increase of the particle diameter.

4.3. Comparison with the experimental data

Experimental results of Elimelech and O'Melia [18] and of Bai and Tien [19] for measuring the collection efficiencies of colloidal particles in a packed bed, are adopted here to compare with the predictions of the present deposition model using PCT, SCT, and HCT, respectively.

In the first study of particle deposition with the presence of the repulsive double layer interactions (i.e., like curve B in Fig. 3), the experimental data reported by Elimelech and O'Melia [18] are adopted. In their experimental work, the collection efficiencies of negatively charged polystyrene latex were determined from the particle deposition experiments in a packed-bed filter, at which the electrolyte concentrations of the suspensions were varied from 0.05 to 0.001 M and the negatively charged glass beads were used as the spherical collectors. In order to consider the Brownian diffusion behavior of particles described in the present paper, only the experimental results of the particle diameter of 0.753 μm are adopted to compare with the above simulation theory. Corresponding to the experimental conditions given in Table 4, the curves of the experimental and theoretical collection efficiencies as a function of electrolyte concentration are presented in Fig. 7. In this figure, the experimental collection efficiency is calculated by the equation

$$\eta_{s\,exp} = 4r_f / \left[3L(1 - \varepsilon) \right] \ln(C_{in}/C_{eff}), \tag{23}$$

where ε is the porosity of the packed-bed filter, L is the length of the packed-bed filter, C_{in} is the influent concentration of the latex particles, and C_{eff} is the effluent concen-

Fig. 7. Comparison of the filter coefficients between the theoretical results and the experimental data obtained from Elimelech and O'Melia [18]. Curve A represents the theoretical predictions when the PCT model is adopted, while curves B and C represent the predictions of using the SCT model and the HCT model, respectively. Curve D is the simulation result obtained by using the convective diffusion model [20]. Curve E shows the predictions obtained by using the correlation equation established by Bai and Tien [19]. Experimental data on the filter coefficients are shown by the symbol of (■).

tration of the latex particles. And the filter coefficient α is defined by the ratio of the initial filter coefficient λ, to its value in the absence of the repulsive energy barrier between two interacting surfaces (i.e., when the ionic strength of the colloidal suspension is high), λ_0, or

$$\alpha = \frac{\lambda}{\lambda_0} = \frac{\eta_s}{\eta_0}. \tag{24}$$

In Fig. 7, curve A is the simulation result of using the PCT model, while curves B and C represent the simulation results of using the SCT model and the HCT model, respectively. The predictions of curve B are almost the same as curve C. Curve D represents the theoretical predictions of the filter coefficient by the convective diffusion model. The complete formulation of this convective diffusion model describing the deposition rates of Brownian particles can be found in detail elsewhere [20]. As described in the dissertation of Rajagopalan [27], when the inertia term of the force balance equation is ignored, there is a direct relationship between the Langevin equation of the present paper and the convective diffusion equation via the Fokker–Planck–Kolmogorov equation and the equivalent form of the Stratonovich differential equation. Curve E represents the correlation equation established by Bai and Tien [19] for estimating the filter efficiency based on four dimensionless parameters, N_{LO}, N_{DL}, N_{E1}, and N_{E2}, as follows:

$$\alpha = 2.527 \times 10^{-3} N_{LO}^{0.7031} N_{E1}^{-0.3121} N_{E2}^{3.5111} N_{DL}^{1.352}. \tag{25}$$

Table 4
Experimental conditions adopted in the study of Elimelech and O'Melia [18]

	KCl (mol/l)	ϕ_p (mV)	ϕ_f (mV)
Exp. 1	0.3	−28.2	−17.5
Exp. 2	0.1	−41.0	−29.3
Exp. 3	0.03	−62.3	−39.0
Exp. 4	0.01	−80.0	−47.5
Exp. 5	0.003	−89.5	−56.4
Exp. 6	0.001	−89.0	−60.0
d_f		200 μm	
d_p		0.753 μm	
U		0.136 cm/s	
L		20 cm	

As shown in this Fig. 7, a common feature of curves A, B, and C is the drastic drop of the filter coefficient when the electrolyte concentration is smaller than 0.01 M. This is caused by an increase in the range of electric double layer repulsion force and the height of the primary energy barrier in the total interaction energy curve as the electrolyte concentration of the solution decreases. This particular electrolyte concentration, 0.01 M, is then referred to as the critical deposition concentration, which demonstrates the unfavorable deposition of particles onto the collector surfaces. Curve D is the convective diffusion model, a drastic drop of the collection efficiency to zero is also observed when the electrolyte concentration of KCl is smaller than 0.1 M. Comparing with the experimental data, it is found that there is a disparity between theory and experiment with respect to the magnitude of the filter coefficient, when the electrolyte concentration is dropped in the unfavorable deposition region. However, since the inertia term is considered in the force balance equation of the present model, hence the filter coefficients of curves A, B, and C are much higher than that of curve D. Therefore, the present model can reduce these differences observed between theoretical predictions and experimental results in the unfavorable deposition region. Also, as shown in Fig. 7, the filter coefficient of curve A is higher than those of curves B and C in this unfavorable deposition region. This result can be explained by the fact that, instead of its higher value of η_s obtained for either SCT or HCT, because of its much higher value of η_0 obtained for these two structures, therefore the filter coefficients of curves B and C are smaller than that of curve A as calculated by using Eq. (24). Curves A, B, C, and D can give good predictions when the electrolyte concentration of KCl is greater than 0.1 M, at which the double layer interactions are attractive. Heterogeneity of surface charge and potential [28], surface roughness [29], and possible additional forces between particles and collectors [30] can be the reason for these well-known discrepancies between the theoretical results and the data measured experimentally, as shown in Fig. 7. Curve E in Fig. 7 indicates that the correlation equation obtained by Bai and Tien [19] fits well with the experimental results of this study.

In the second study, the experimental data obtained by Bai and Tien [19] are compared with the predictions of the present deposition model. In this experiment, the collection efficiencies of polystyrene latex of various sizes through a Bollotini glass beads packed column were measured, and the experimental condition is listed in Table 5. The typical sets of experimental results are shown in Fig. 8, while the diameter of latex is 0.802 μm and the double layer interaction force is repulsive. It is found that the filter coefficient α increase with the increase of ionic concentration (i.e., because of the compression of the double layer thickness), and the values of α are as high as 1.0 when the concentration of NaCl is at 0.1 M. This coincides with Fig. 7, where both curves A, B, and C show discrepancies between predictions and experimental data at the unfavorable deposition region

Table 5
Experimental conditions adopted in the study of Bai and Tien [19]

	NaCl (mol/l)	ϕ_p (mV)	ϕ_f (mV)	d_p (μm)
Exp. 1	0.0001	−20.7	−22.8	0.802
Exp. 2	0.001	−19.3	−21.2	0.802
Exp. 3	0.01	−15.7	−18.1	0.802
Exp. 4	0.1	−7.0	−11.2	0.802
U		0.103 cm/s		
d_f		460 μm		
L		10.3 cm		
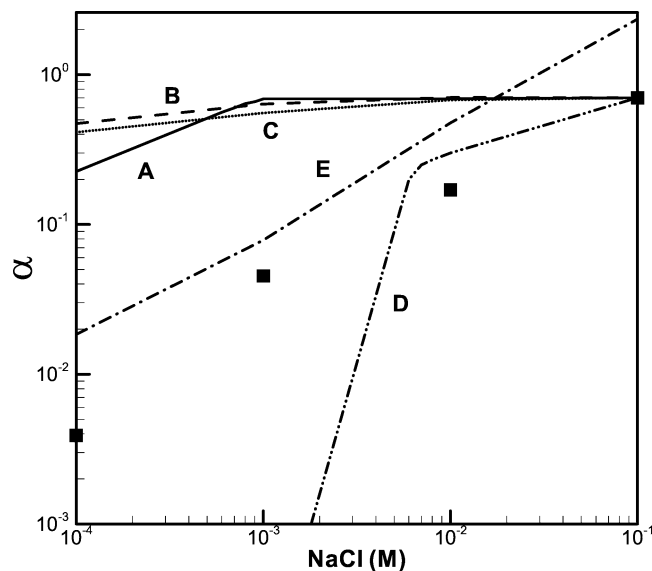
Fig. 8. Comparison of the filter coefficients between the theoretical results and the experimental data obtained from Bai and Tien [19]. Curve A represents the theoretical predictions when the PCT model is adopted, while curves B and C represent the predictions of using the SCT model and the HCT model, respectively. Curve D is the simulation result obtained by using the convective diffusion model [20]. Curve E shows the predictions obtained by using the correlation equation established by Bai and Tien [19]. Experimental data of the filter coefficients are shown by the symbol of (■).

of low electrolyte concentrations. Since those particles at the entrance of the tube will collide with the tube wall immediately in the present model, curves A, B, and C overestimate the collection efficiencies of particles when the concentration of NaCl is smaller than 0.1 M. Different with what obtained in the theoretical simulations of Fig. 7, the α values of curves B and C are slightly higher than that of curve A when the concentration of NaCl is smaller than 0.01 M. As mentioned above, curve D is the simulation result obtained when the convective diffusion model is adopted. Except in the unfavorable deposition region, curve D coincides well with the experimental data when the concentration of NaCl is greater than 0.01 M, at which the interaction forces are attractive and the collection efficiencies of particles are very high. Also, it is found that Bai and Tien's predicted α values shown by curve E are slightly higher than those of experimental results in Fig. 8.

5. Conclusion

By assuming that the constricted tube model characterizes the filter bed, the deposition behavior of colloidal particles is investigated by using the Brownian dynamics simulation method in the present paper. The contributions of different constricted tube structures, PCT, HCT, and SCT, various shapes of the total interaction energy curves and the different particle diameters, to the collection efficiencies of Brownian particles are examined. The simulation results show that the height of the primary maximum and the depth of the secondary minimum in the total interaction energy curve of DLVO theory play an important role in determining the collection efficiency of the Brownian particles. When comparing the values of the collection efficiencies at different Reynolds numbers among these three tube structures, we found that SCT > HCT > PCT in general for those interaction energy curves with different primary maximum heights and secondary minimum depths, and *vice versa* for the curve without any energy barrier. When comparing with the available experimental data of measuring the filter coefficient, we found that the present model can give a discrepancy between theoretical predictions and experimental data smaller than that of the convective diffusion model in the unfavorable deposition region.

Because the present model only considers the initial deposition behavior of Brownian particles and is deficient in describing the multilayer adsorption behavior of particles, it cannot predict the collection efficiency at the unfavorable deposition region well. According to the theoretical model established by Choo and Tien [31], when the degree of multilayer adsorption of particles and cake formation at the tube entrance is taken into account, the extent of deposition of particles goes through a three-stage deposition process: individual deposition on the pore surface, multilayer deposition, and the formation of a deposit layer at the tube entrance. Therefore, in order to describe the particle deposition behavior in a more realistic way, the model of the present paper will incorporate the three-stage deposition process in our future work.

Acknowledgment

Appendix A. Nomenclature

A	Hamaker constant
$A(t)$	Gaussian white noise process in stochastic terms
d_c	constriction diameter
C_{in}	influent particle concentration
C_{eff}	effluent particle concentration
d_c	constriction diameter of a constricted tube
d_f	filter-grain diameter
d_{max}	maximum diameter of constricted tube
d_p	diameter of particle
$F_1(H), F_2(H), F_3(H)$	retardation factors of normal vector, drag force, and shear vector, respectively
F_{DL}	dimensionless electrostatic repulsion force, defined by Eq. (21)
F_{LO}	dimensionless van der Waals force, defined by Eq. (20)
H	defined as h_s/r_p
h	height of constricted tube
h_s	the smallest separation distance between the particle and the collector surface
k_B	Boltzmann constant
L	length of the filter bed
l_f	length of the unit bed element
m_p	mass of the particle
N_c	number of unit cells per unit cross-sectional area
N_{dep}	number of particles deposited
N_{DL}	double-layer force parameter, defined as κr_p
N_{E1}	first electrokinetic parameter, defined as $$v r_p \left(\varphi_1^2 + \varphi_2^2\right)/4 k_B T$$
N_{E2}	second electrokinetic parameter, defined as $$2\left(\frac{\varphi_1}{\varphi_2}\right) \Bigg/ \left[1 + \left(\frac{\varphi_1}{\varphi_2}\right)^2\right]$$
N_{gen}	number of particles generated at tube inlet
N_{LO}	defined as $A/6 k_B T$
N_{Re}	Reynolds number, defined as $u_s d_f \rho_f / \mu$
$N_{Re,m}$	Reynolds number, defined as $u_m r_m \rho_f / \mu$
$P(y_0)$	initial deposition rate of Brownian particles
R	defined as r/r_w
R_m	defined as r_m/l_f
$R_v(t)$	random deviates of velocity increment due to Brownian motion, which are bivariate Gaussian distribution
$R_r(t)$	random deviates of displacement increment due to Brownian motion, which are bivariate Gaussian distribution
R_w	defined as $R_w = r_w/r_m$
r_0	remotest radial position at the constriction tube inlet which can be reached by a particle
r_c	constriction radius
r_f	filter-grain radius
r_{in}	radial coordinate of the particle position at tube inlet

r_m	defined as $1/l_f \int_0^{l_f} r_w \, dz$
$r_{\max}$	maximum radius of constriction tube
r_w	wall radius
S	position vector
S_0	initial value of S
S_{wi}	fraction of saturation
T	absolute temperature
t	time
U	uniform velocity entering constriction tube
u_m	average axial velocity across the constriction in a constricted tube
u_r	velocity component along the radius direction
$u_{r0}^*, u_{r1}^*, u_{r2}^*$	the zeroth, first, and second dimensionless expressions of u_r, defined by Eqs. (10), (11), and (12), respectively
u_s	superficial velocity
u_z	velocity component along the axial direction
$u_{z0}^*, u_{z1}^*, u_{z2}^*$	the zeroth, first, and second dimensionless expressions of u_z, defined by Eqs. (13), (14), and (15), respectively
V	particle velocity vector
V_0	initial velocity of V
Z	particle position vector
Z_0	initial value of Z

Greek symbols

α	filter coefficient, defined by Eq. (24)
β	friction coefficient per unit mass of particle
ε	filter porosity
ϕ_{DL}	dimensionless van der Waals attractive energy
ϕ_{LO}	dimensionless electrostatic repulsive energy
φ_1, φ_2	surface (zeta) potentials of particle and collector, respectively
η_0	value of η_s under favorable surface interaction
η_s	initial deposition rate of Brownian particles
$\eta_{s\,\exp}$	experimental data of η_s
θ_{in}	angular coordinate of the particle position at tube inlet
κ	reciprocal of the electric double layer thickness
λ	initial filter coefficient
λ_0	initial value of λ under favorable surface interaction
μ	viscosity of fluid
ν	dielectric constant of the fluid
ρ_f	density of fluid

ψ	stream function
$\psi_0^*, \psi_1^*, \psi_2^*$	the zeroth, first and second order solutions of stream functions, defined by Eqs. (4), (5), and (6), respectively.

Other symbols

$\langle \; \rangle$	average value
∇	gradient operator

References

[1] C. Tien, A.C. Payatakes, AIChE J. 25 (1979) 737.
[2] C. Tien, Granular Filtration of Aerosols and Hydrosols, Butterworhts, Boston, 1989, Chapters 3–5.
[3] L.A. Spielman, J.A. FitzPatrick, J. Colloid Interface Sci. 42 (1973) 607.
[4] A.C. Payatakes, R. Rajagopalan, C. Tien, Can. J. Chem. Eng. 52 (1974) 722.
[5] C.C. Hung, C. Tien, Desalination 18 (1976) 173.
[6] K.M. Yao, M.T. Habidian, C.R. O'Melia, Environ. Sci. Technol. 5 (1971) 1105.
[7] R. Rajagopalan, C. Tien, Can. J. Chem. Eng. 55 (1977) 246.
[8] R. Vaidyanathan, C. Tien, Chem. Eng. Sci. 43 (1988) 289.
[9] R. Rajagopalan, C. Tien, AIChE J. 22 (1976) 523.
[10] R.I. Mackie, R.M.W. Horner, R.J. Jarvis, AIChE J. 33 (1987) 1761.
[11] A.C. Payatakes, C. Tien, R.M. Turian, AIChE J. 19 (1973) 58.
[12] C. Kanaoka, H. Emi, W. Tarthapanichakoon, AIChE J. 29 (1983) 895.
[13] D. Gupta, M.H. Peters, J. Colloid Interface Sci. 104 (1985) 375.
[14] B.V. Ramarao, C. Tien, S. Mohan, J. Aerosol Sci. 25 (1994) 295.
[15] Y.I. Chang, J.J. Whang, Chem. Eng. Sci. 53 (1998) 3923.
[16] Y.I. Chang, S.C. Chen, D.K. Chern, Sep. Purif. Technol. 27 (2002) 97.
[17] E.J.W. Verwey, J.Th.G. Overbeek, Theory of the Stability of Lyophobic Colloids, Elsevier, Amsterdam, 1948.
[18] M. Elimelech, R.C. O'Melia, Langmuir 6 (1990) 1153.
[19] R. Bai, C. Tien, J. Colloid Interface Sci. 218 (1999) 488.
[20] D.C. Prieve, E. Ruckenstein, AIChE J. 20 (1974) 1178.
[21] P. Fedkiw, J. Newman, AIChE J. 23 (1977) 255.
[22] M. Venkatesan, R. Rajagopalan, AIChE J. 26 (1980) 694.
[23] H. Pendse, C. Tien, AIChE J. 28 (1982) 677.
[24] J.C.F. Chow, K. Soda, Phys. Fluids 15 (1972) 1701.
[25] H.W. Chiang, C. Tien, AIChE J. 31 (1985) 1349.
[26] R. Rajagopalan, J.S. Kim, J. Colloid Interface Sci. 83 (1981) 428.
[27] R. Rajagopalan, Stochastic Modeling and Experimental Analysis of Particle Transport in Water Filtration, Ph.D. dissertation, Syracuse University, Syracuse, New York, 1974, Chapters 4–6.
[28] J. Stankovich, S.L. Carnie, J. Colloid Interface Sci. 216 (1999) 329.
[29] Y.I. Rabinovich, J.J. Adler, A. Ata, R.K. Singh, B.M. Moudgil, J. Colloid Interface Sci. 232 (2000) 17.
[30] J. Israelachvili, Intermolecular and Surface Forces, 2nd ed., Academic Press, New York, 1997, Chapters 13 and 14.
[31] C.U. Choo, C. Tien, AIChE J. 41 (1995) 1426.